micro

MDPI

Article

Laser-Surface-Remelted Powder Metallurgy TiAl Alloys: Microstructure and Mechanical Properties

Warlen Monfardini [1], João Victor Vieira [2], João Batista Fogagnolo [2] and Juliano Soyama [2,*]

[1] School of Mechanical Engineering, Federal Institute of Espírito Santo, Morobá Street 248, Aracruz 29192-733, ES, Brazil; warlen.monfardini@ifes.edu.br
[2] School of Mechanical Engineering, University of Campinas, Mendeleyev Street 200, Campinas 13083-860, SP, Brazil; j174769@dac.unicamp.br (J.V.V.); fogagnol@unicamp.br (J.B.F.)
* Correspondence: jsoyama@unicamp.br

Abstract

Laser processing has been widely investigated as an effective approach for improving surface properties and consolidating advanced materials, particularly complex alloys such as titanium aluminides (TiAl). In this study, laser surface remelting was applied to binary (Ti-45Al) and ternary (Ti-45Al-2Co and Ti-45Al-2Ni) alloys produced by powder metallurgy via blended elemental (BE) and pre-alloyed (PA) powder routes. Laser powers of 50 and 100 W were employed, resulting in a high-energy-density surface remelting regime applied to both green compacts and sintered samples with relatively high initial porosity, under an argon-controlled atmosphere. Microstructural and phase analyses were performed using scanning electron microscopy (SEM) and X-ray diffraction (XRD), while mechanical behavior was assessed by instrumented microindentation. Laser processing promoted the formation of a dense and homogeneous surface layer, approximately 150 µm thick, accompanied by significant microstructural refinement and enhanced hardness and elastic modulus. While rapid solidification led to crack formation in laser-treated sintered samples, the green compacts exhibited defect-free modified layers. Overall, the results demonstrate that laser surface remelting is an effective strategy for enhancing the surface integrity and mechanical performance of TiAl alloys processed by powder metallurgy.

Keywords: powder metallurgy; laser surface remelting; TiAl; surface densification

1. Introduction

For more than two decades, laser-based processing has been extensively investigated as an effective approach for both consolidation and surface modification of titanium aluminides (TiAl) [1]. In particular, significant progress has been achieved within the framework of additive manufacturing (AM), which has undergone rapid development since the early 2010s [2]. Numerous successful applications have been reported, especially for powder-based technologies such as Direct Energy Deposition (DED) [3,4] and Powder Bed Fusion (PBF) [5–8].

In DED processes, a focused energy source is employed to melt and consolidate material supplied either in powder or wire form [9]. PBF technologies, originally derived from selective laser sintering concepts developed in the late 1980s, have since evolved into several variants, including Selective Laser Melting (SLM) and Electron Beam Melting (EBM). Despite their differences, these techniques share a common operating principle, consisting of the layer-by-layer melting of powder beds using a concentrated energy source

Academic Editor: Zhou Li

Received: 12 February 2026
Revised: 2 March 2026
Accepted: 15 March 2026
Published: 17 March 2026

to produce complex three-dimensional geometries, with powder recoating performed after each processing cycle [2–9].

Although a substantial portion of the literature has focused on laser-based manufacturing routes, laser processing has also proven to be highly effective for a wide range of surface modification techniques, including surface remelting, surface alloying, cladding [10], and laser surface polishing [11]. These laser-induced surface modifications are commonly associated with significant improvements in material performance, such as enhanced wear and corrosion resistance, pronounced microstructural refinement, increased hardness, and improved biocompatibility [10,11].

Compared with more conventional surface treatments, including thermochemical processes (e.g., carburizing and boriding) and thermal spray techniques, laser-based surface modification offers several advantages, notably higher processing precision, reduced thermal impact on the substrate, shorter processing times, and the formation of a strong metallurgical bond between the modified layer and the underlying material [10]. Other surface modification techniques such as electric spark alloying (ESA) have been reported to provide highly localized thermal effects with minimal overall heat input due to the pulsed nature of the spark discharge. As a result, the thermal impact zone generated during ESA can be significantly smaller than in laser- or arc-based treatments, reducing the risk of substrate deformation and enabling localized surface modification [12,13].

TiAl, primarily composed of the γ(TiAl) and α_2(Ti_3Al) phases, are technologically important intermetallic alloys for high-temperature structural applications, such as low-pressure turbine blades and high-pressure compressor components, owing to their attractive combination of properties. These include the ability to operate at temperatures above 900 °C, high oxidation and corrosion resistance, and an excellent strength-to-density ratio [14,15].

Despite these advantages, Ti-Al alloys, similar to other titanium-based intermetallic systems, exhibit intrinsically low room-temperature ductility and are associated with high processing costs, which significantly limit their widespread industrial adoption [14–17]. In powder metallurgy routes, additional challenges arise during sintering, including the Kirkendall effect, volumetric swelling associated with the formation of intermediate intermetallic compounds (e.g., $TiAl_3$ and $TiAl_2$), and the inherently low compressibility of PA powders when such starting materials are employed [18–22].

In this context, laser processing, even when applied as a thin surface treatment, presents considerable potential to overcome some of these limitations. Laser-induced melting can promote the dissolution of non-diffused elements, induce microstructural refinement, and, most importantly, enhance the surface densification of sintered materials. Recent studies have reported promising results using laser-based approaches for Ti-Al alloys, as well as for pure Ti and Ti-6Al-4V systems [8,11,23–26]. Notably, Yan et al. [25] demonstrated that, when compared with advanced sintering techniques such as spark plasma sintering (SPS) and hot pressing (HP), SLM produced superior mechanical properties, highlighting the effectiveness of laser-matter interaction even relative to state-of-the-art consolidation routes.

Another increasingly relevant application of laser processing is related to intentional compositional modification of surfaces, either through laser alloying [27] or laser-assisted coating techniques [28]. In this context, Zhang et al. published a comprehensive review addressing the state of the art and the main challenges associated with laser-induced compositional tailoring [29]. In addition, the development of stiffness and hardness gradients achieved by laser surface remelting has attracted growing attention [30], particularly for biomedical applications, where graded mechanical responses are desirable to improve load transfer and interfacial compatibility.

Despite the numerous advantages associated with laser-based surface treatments, the inherently high cooling rates can strongly influence grain morphology, promote the development of significant residual stresses, and, in some cases, lead to crack formation. Moreover, the elevated temperatures reached during laser processing may induce substantial compositional variations, such as aluminum evaporation in Ti-Al-based alloys [1–11,23,25]. In this regard, Gussone et al. [8] demonstrated that substrate preheating plays a key role in reducing thermal gradients and cooling rates, thereby mitigating residual stresses and associated defects.

Although a substantial body of literature addresses the production of components by laser-based techniques, studies specifically focused on laser surface processing using different combinations of PA and elemental powders remain comparatively limited for TiAl. In this context, the objective of the present work is to evaluate the influence of laser surface remelting on the densification behavior, phase constitution, and mechanical response of powder-metallurgy Ti-Al alloys processed via distinct powder routes, in both green and sintered conditions.

2. Materials and Methods

2.1. Material Preparation

Three Ti-Al-based compositions were investigated in this study: a binary Ti-45Al alloy and two ternary alloys, Ti-45Al-2Co and Ti-45Al-2Ni (at.%). The materials were produced by powder metallurgy using two different powder routes: blended elemental (BE) and pre-alloyed (PA).

For the BE route, commercially pure Ti, Al, and Co powders supplied by Stanford Advanced Materials (Irvine, CA, USA), all with nominal purities of 99.9% and particle sizes below 40 μm, were used. Nickel powder supplied by Synth (São Paulo, Brazil) presented a purity of 99.5% and particle sizes in the range of 7.5–10.5 μm. For the PA route, a commercially available Ti-50Al PA powder supplied by Alfa Aesar (Haverhill, MA, USA), with a purity of 99.5% and a particle size below approximately 45 μm, was employed. In this case, the nominal composition was adjusted to Ti-45Al by the addition of elemental titanium during the powder mixing stage. For the ternary alloys, cobalt or nickel powders were subsequently added to the powder blends.

All powders were mixed according to the target compositions to ensure chemical homogeneity prior to compaction. The powder blends were uniaxially compacted into cylindrical specimens using a die with a diameter of 8.1 mm, under a compaction pressure of 390 MPa.

After compaction, the samples were divided into two conditions. One set was subjected to sintering at 1300 °C for 2 h under an argon atmosphere using a resistive tubular furnace (Grion, São Paulo, Brazil), while the remaining specimens were kept in the as-compacted (green) state. The relative densities of the sintered samples were subsequently evaluated by image analysis. Both green and sintered samples were then used for further processing and characterization. Prior to laser processing, the sintered samples underwent surface preparation by sanding with #600 SiC sandpaper, followed by cleaning and drying, whereas the green compacts were directly subjected to laser surface treatment in the as-compacted condition, without additional surface preparation.

All powders were stored and handled inside an argon-filled glovebox to minimize atmospheric contamination. A schematic representation of the sample preparation and consolidation route is provided in Figure 1.

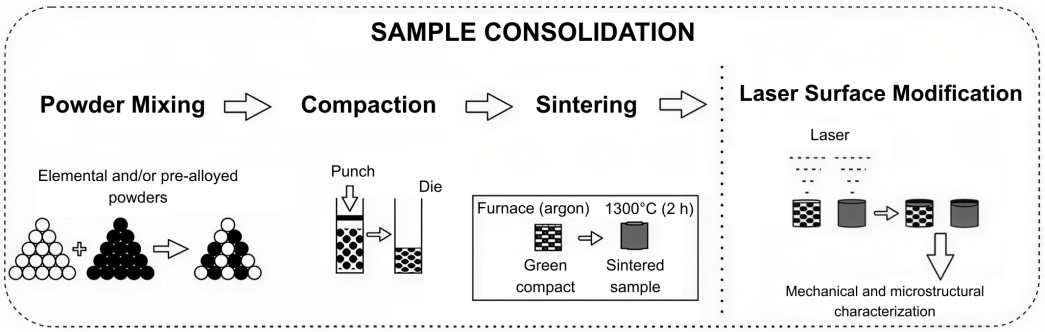

Figure 1. Schematic representation of the powder metallurgy processing routes (BE and PA), followed by uniaxial compaction and subsequent division into green compacts and sintered samples, laser surface remelting applied exclusively to the top surface, and final microstructural and mechanical characterization.

2.2. Laser Processing

The laser surface remelting experiments were carried out using an ytterbium-doped fiber laser (model YLR-500MM-AC-Y11, IPG Photonics, Oxford, MA, USA), operating at a wavelength of 1070 nm. All laser treatments were conducted under an argon-controlled atmosphere (99.9% purity) in order to minimize oxidation during processing.

The laser beam was scanned over the sample surface following a zigzag movement strategy, similar to that reported by Thijs et al. [31], using a computer numerical control (CNC)-driven positioning system. The laser was applied exclusively to the top surface of the specimens.

The main laser processing parameters are summarized in Table 1. Based on the selected processing conditions, the volumetric energy density E was estimated using Equation (1) [32], which relates laser power P, scan speed v, hatch distance h, and remelted layer thickness t:

$$E = \frac{P}{v \cdot h \cdot t} \quad (1)$$

Table 1. Laser surface remelting processing parameters used in this study.

Parameter	Symbol	Unit	Value
Laser power	P	W	100
Scan speed	v	mm·min^{-1}	600
Hatch distance	h	µm	175
Focal distance	–	mm	42
Beam diameter	–	mm	0.5
Shielding gas	–	–	Argon
Shielding gas flow rate	–	L·min^{-1}	10

Under the conditions employed with a laser power of 100 W, the process operated in a high-energy-density surface remelting regime, with estimated energy densities on the order of 380 J·mm^{-3}, associated with the formation of remelted layers approximately 150 µm thick. In selected experiments, a reduced laser power of 50 W was also investigated, resulting in thinner remelted layers with thicknesses on the order of 50 µm.

2.3. Microstructural and Mechanical Characterization

Microstructural characterization was carried out by scanning electron microscopy (SEM) using a Zeiss EVO MA15 microscope (Carl Zeiss, Oberkochen, Germany) equipped with an energy-dispersive spectroscopy (EDS) detector (Oxford Instruments, Abingdon, UK). Phase identification was performed by X-ray diffraction (XRD) using an X'Pert^3

PRO Powder diffractometer (Malvern Panalytical, Malvern, UK) with Cu-Kα radiation, operating at an accelerating voltage of 40 kV and a tube current of 30 mA.

Mechanical properties were evaluated by instrumented microindentation tests, from which hardness and elastic modulus values were obtained. The tests were conducted using an MHT^3 microindenter (Anton Paar, Graz, Austria) mounted on a Step 700 surface analysis platform. Data acquisition and analysis were performed using the Indentation 9.0.12 software. A Berkovich-type diamond indenter was employed, following the methodology proposed by Oliver and Pharr [33]. Indentations were performed with a maximum load of 300 mN, using loading and unloading rates of 1000 mN·min^{-1}, and a holding time of 15 s at peak load. For each condition, five indentations were performed in representative regions of the analyzed surface. In the case of laser-treated samples, measurements were carried out within the remelted zone. The reported values correspond to the mean ± standard deviation.

The Poisson's ratios of the tested material and the indenter were taken as 0.29 and 0.07, respectively. The resulting load–displacement curves were analyzed in accordance with ASTM E2546 [34] and ASTM B933 [35].

3. Results and Discussion

3.1. Powder Characterization

Table 2 summarizes the particle size distribution of the powders used in this study, while Figure 2 presents their morphological features along with the corresponding EDS spectra. The aluminum powder exhibited a predominantly spherical morphology, whereas the titanium and TiAl (γ) powders showed irregular particle shapes. In the case of the PA powder, the particles appeared mainly as agglomerates, with a median size (D_{50}) of approximately 75 μm.

Table 2. Particle size distribution of the powders used in this study.

Parameter [1]	Ti	Al	TiAl [2]	Co	Ni
D_{10} (μm)	6.63	13.01	22.03	6.12	6.45
D_{50} (μm)	16.92	25.22	75.35	12.64	13.49
D_{90} (μm)	42.28	40.87	119.88	26.29	25.59

[1] D_{10}, D_{50}, and D_{90} correspond to the cumulative particle sizes at 10%, 50%, and 90%, respectively. [2] Agglomerate size.

The cobalt and nickel powders were also examined by SEM and exhibited predominantly spherical morphologies, with the presence of some satellite particles, similar to those observed for the aluminum powder.

The particle size distribution data indicate that the elemental powders (Ti, Al, Co, and Ni) exhibited narrower size ranges compared to the PA TiAl powder, whose distribution reflects its agglomerated nature. As indicated in Table 2, the reported D_{10}, D_{50}, and D_{90} values correspond to the cumulative particle sizes at 10%, 50%, and 90%, respectively, while the values reported for the TiAl powder represent agglomerate sizes.

XRD analysis confirmed the presence of equilibrium phases in the powders. The Ti powder exhibited a hexagonal close-packed (hcp) crystal structure corresponding to the α-Ti phase, the TiAl powder showed a tetragonal structure associated with the γ-TiAl phase, and the Al powder presented a face-centered cubic (fcc) structure.

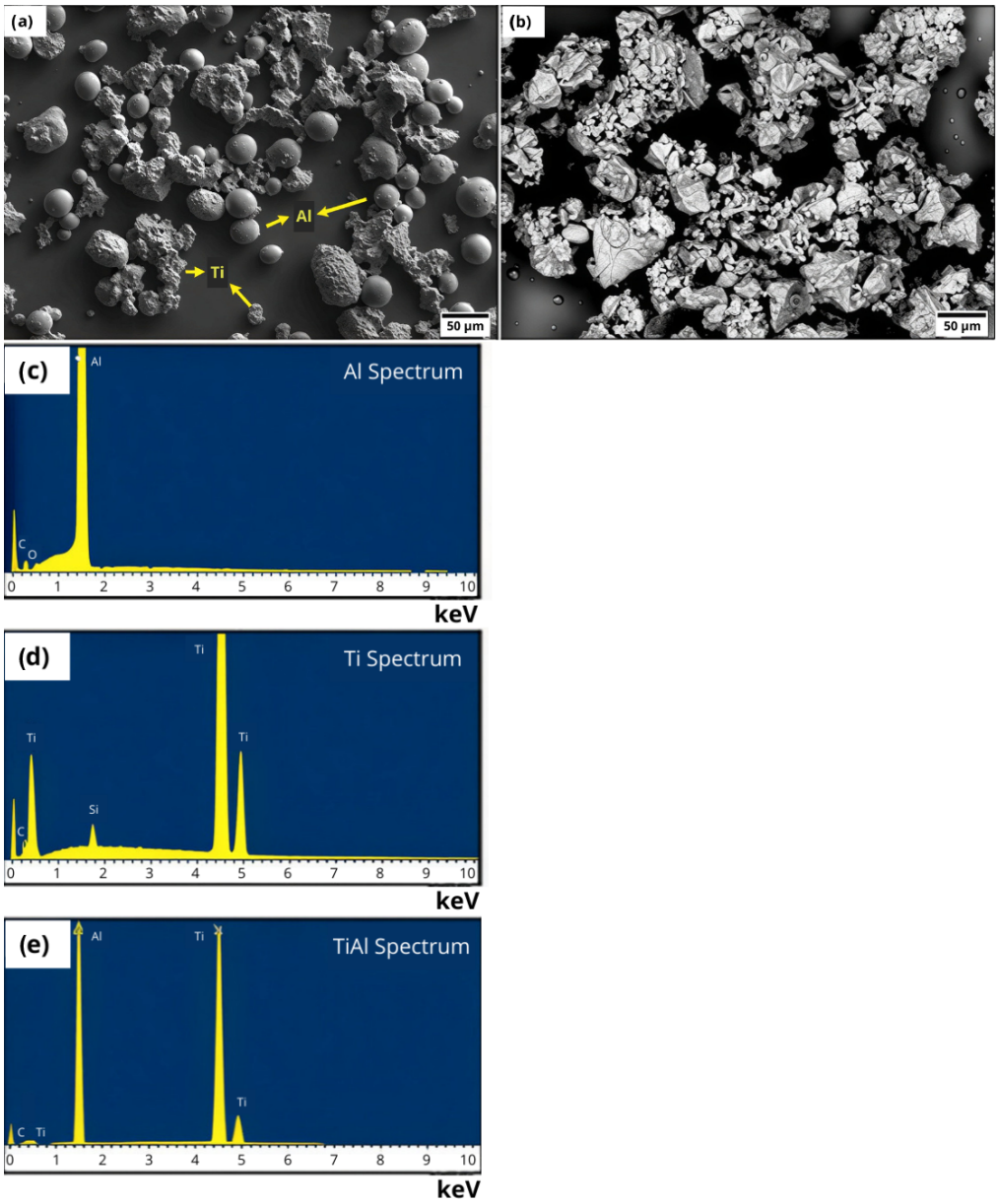

Figure 2. SEM micrographs showing the morphology of (**a**) BE Ti and Al powders and (**b**) PA TiAl powders. Corresponding EDS spectra of (**c**) Al, (**d**) Ti, and (**e**) TiAl powders.

3.2. Microstructural Characterization of As-Processed and Laser-Modified Samples

3.2.1. Green Compacts and Sintered Samples

The SEM micrographs presented in Figure 3 illustrate the microstructures of the binary Ti-45Al alloys processed by powder metallurgy using BE and PA powder routes, in both the as-compacted (Figure 3a,c) and sintered conditions (Figure 3b,d), respectively.

In the green compacts (Figure 3a,c), the microstructures reflect the morphology and packing characteristics of the starting powders, with limited interparticle bonding and a high level of porosity. After sintering, distinct microstructural features were observed depending on the powder route. The BE Ti-45Al alloy (Figure 3b) exhibited a duplex microstructure, whereas the PA Ti-45Al alloy (Figure 3d) showed a fully lamellar microstructure, both consisting of equilibrium phases formed during slow cooling. These transformations are associated with diffusional reactions of the type $\alpha(Ti) \rightarrow \alpha_2(Ti_3Al) + \gamma(TiAl)$ as reported in the literature [14,16,17].

Despite the microstructural development promoted by sintering, a relatively low degree of densification was achieved in both materials, as evidenced by the presence of

numerous large, irregular, and partially interconnected pores. Such porosity is characteristic of the early and intermediate stages of solid-state sintering. Similar microstructural features and density levels have been reported in previous studies and are commonly attributed to: (i) the limited compressibility of PA powders; (ii) swelling effects associated with the formation of intermediate intermetallic phases (e.g., $TiAl_2$ and $TiAl_3$); and (iii) the significant difference in diffusion rates between Ti and Al, leading to Kirkendall porosity [18,20–22,36–38].

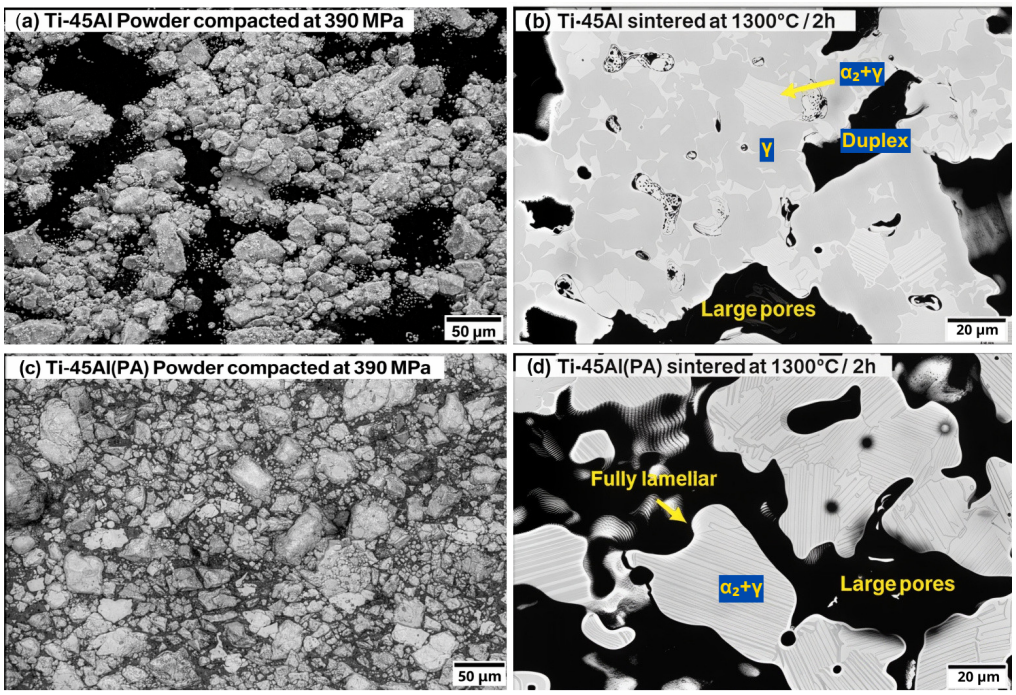

Figure 3. SEM micrographs of Ti-45Al alloys processed by powder metallurgy: compacted samples produced from BE (**a**) and PA powders (**c**), and sintered samples obtained from the same powder routes (**b**,**d**), prior to laser surface modification.

In addition to these factors, the sintering parameters were not optimized for high densification, since the present study aimed to evaluate laser surface remelting under representative processing conditions. Thus, the relatively high porosity was expected and useful for assessing the effectiveness of the laser treatment in promoting localized densification.

The relative density values measured for the green compacts and sintered samples are summarized in Table 3. A decrease in densification after sintering was observed for the BE alloy, which can be associated with the porosity formation mechanisms previously mentioned, including intermetallic swelling and diffusion-induced porosity. In addition, green density was determined geometrically using Archimedes' principle, whereas sintered density was estimated by image analysis, which may also contribute to differences in the measured values.

Table 3. Relative density values of green and sintered Ti-45Al samples obtained by Archimedes' principle and image analysis.

Condition	Green Density [1] (%)	Sintered at 1300 °C/2 h [2] (%)
Ti-45Al	73.38 ± 2.21	58.28 ± 3.47
Ti-45Al (PA)	59.05 ± 0.88	69.21 ± 4.33

[1] Density measured by the Archimedes' principle [39]. [2] Density measured by image analysis using ImageJ software (version 1.54a, National Institutes of Health, Bethesda, MD, USA).

3.2.2. Laser Surface Modification

Figure 4, obtained by optical microscopy, illustrates top and cross-sectional views of laser-modified sintered Ti-45Al samples, highlighting the effect of different laser powers on the modified layer morphology. The applied energy input was sufficiently high to induce melting of surface layers with thicknesses ranging from approximately 50 to 150 µm, depending on the processing conditions.

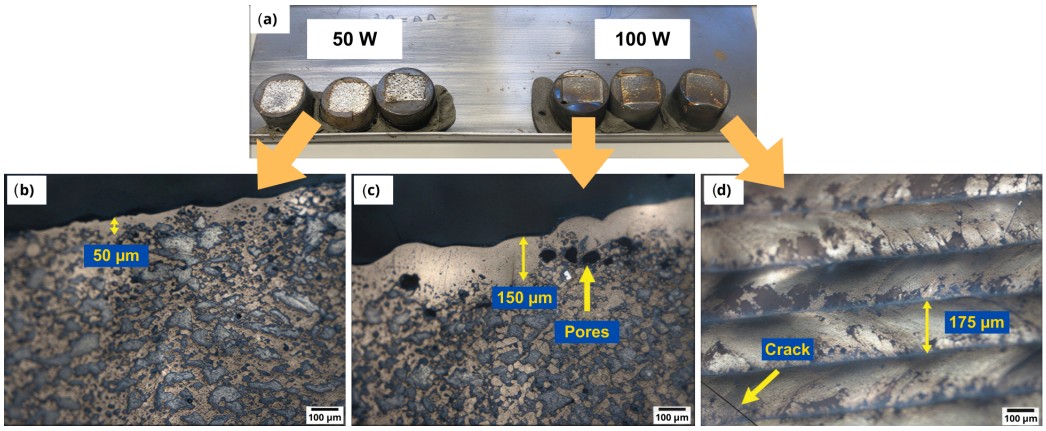

Figure 4. Optical micrographs showing top views (**a**,**d**) and cross-sectional views of laser-modified layers produced at 50 W (**b**) and 100 W (**c**) on sintered Ti-45Al samples. Typical features such as melt pool depth, pores, and cracks are highlighted.

The presence of cracks and residual porosity within the remelted layers can be observed, which is primarily attributed to the high cooling and solidification rates imposed by the laser process. These features are commonly reported on laser-based processing routes and are frequently associated with the development of residual thermal stresses [5,7–11,23,25].

Previous studies have also indicated that substrate preheating may represent an effective strategy to mitigate residual stresses [9,23] and, in some cases, to promote controlled grain orientation and texture development [40]. However, preheating was not possible in the experimental setup employed in this work.

Despite the presence of pores and cracks, as observed in the SEM micrographs shown in Figure 5, the laser-modified layers exhibit a significantly higher level of densification and microstructural homogeneity compared to the adjacent material. This improvement is mainly associated with the melting induced by laser irradiation, which promotes enhanced mass transport and pore elimination due to the transition to the liquid state.

The solidification path of these alloys resembles that reported for SLM processes, involving transformations such as $L \rightarrow L + \beta \rightarrow \beta + \alpha \rightarrow \alpha \rightarrow \alpha_2 + \gamma$ [7,14,41]. In addition to the eutectoid reaction ($\alpha \rightarrow \alpha_2 + \gamma$), typically observed during conventional sintering, other transformations may occur under rapid solidification conditions, including the peritectic reaction ($L + \beta \rightarrow \alpha$). Minor variations in aluminum content can therefore lead to significant differences in the resulting solidification microstructures and textures [14], particularly considering the tendency for Al evaporation at elevated temperatures.

Although the β phase is not present in the equilibrium Ti-Al phase diagram, its formation may be promoted by the presence of β-stabilizing elements such as Nb, Mo, Co, Ni, etc. [7,14,23,40].

Additionally, Figure 5e,f indicate that laser modification promotes effective dilution of ternary elements in both green compacts and sintered samples. While Co particles and Ni-rich segregated regions are observed outside the laser-modified layer, such features are not

detected within the remelted surface region, indicating improved chemical homogeneity after laser processing.

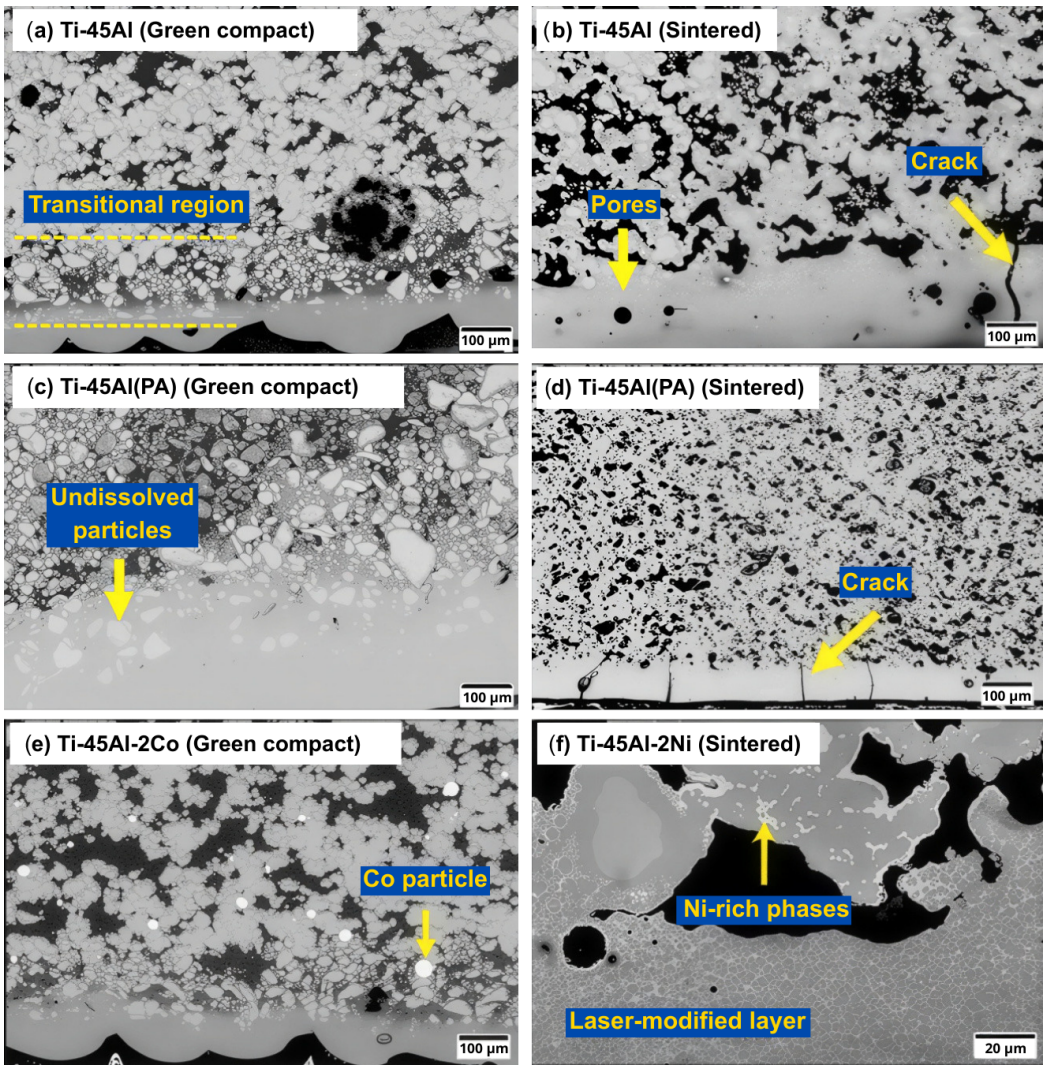

Figure 5. SEM micrographs of laser-modified Ti-45Al-based samples: (**a**,**c**,**e**) correspond to green compacts, while (**b**,**d**,**f**) represent sintered samples. Key microstructural features, including pores, cracks, undissolved particles, elemental segregation, and the laser-modified layer, are indicated.

When comparing the laser-modified layers of sintered samples (Figure 5b,d,f) with those obtained from green compacts (Figure 5a,c,e), a higher density of pores and cracks is observed in the sintered condition. This behavior can be attributed to the increased mobility of particles in the unsintered state, which promotes more effective accommodation of thermally induced stresses during rapid heating and solidification, thereby mitigating the formation of structural defects.

Figure 6 presents the results of the EDS analysis performed on laser-modified Ti-45Al green compacts, revealing a relatively homogeneous distribution of Ti and Al throughout the modified layer. No significant aluminum depletion was detected under the investigated processing conditions, indicating that Al evaporation or other compositional losses were minimal. For the BE samples (Figure 6a), intermediate intermetallic compounds, such as $TiAl_2$ and $TiAl_3$, were identified within the transition region adjacent to the laser-modified layer, indicating incomplete interdiffusion prior to laser processing. These features are no longer observed within the remelted surface region, suggesting that laser treatment effectively promotes chemical homogenization.

Figure 7 evidences the presence of a pronounced microstructural gradient across the laser-modified region of the sintered samples, arising from the steep thermal gradient and variations in cooling rate as the distance from the laser-affected surface increases. Columnar grains are observed in the outermost region of the modified layer, preferentially aligned along the heat flow direction, whereas regions farther from the surface retain a duplex microstructure inherited from the prior sintering conditions. Similar microstructural transitions, driven by spatial variations in solidification conditions, have been widely reported in both direct metal deposition [4] and laser surface fusion processes [6,7,9,11].

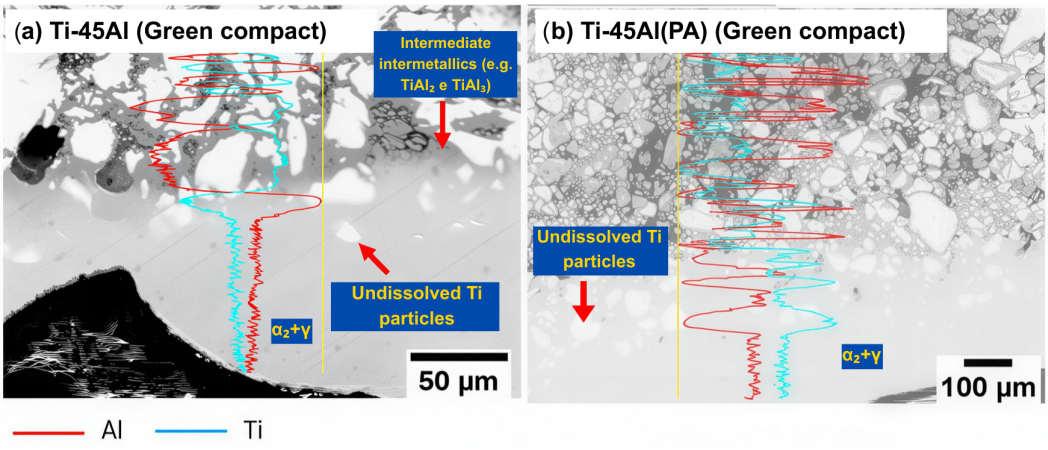

Figure 6. SEM micrographs showing the elemental distribution of Ti and Al obtained by EDS line-scan analysis across the laser-modified layers in green compacts (**a**) and sintered Ti-45Al samples (**b**).

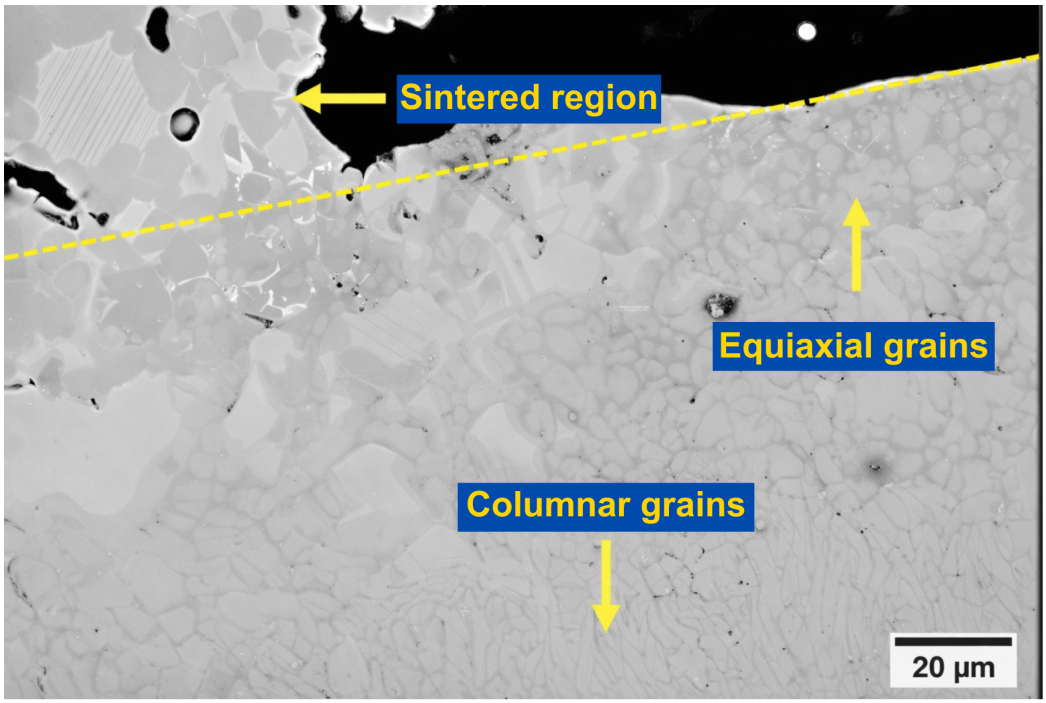

Figure 7. SEM micrograph showing the microstructural gradient across the laser-modified layer and the adjacent substrate region. The yellow dashed line indicates the approximate boundary between the laser-modified layer and the substrate.

3.3. Phase Formation Analysis

Based on the XRD results shown in Figure 8, the consolidation of the equilibrium α_2 and γ phases after sintering was confirmed for the binary Ti-45Al alloys produced from both BE and PA powders. However, conventional sintering was not fully effective in dissolving residual elemental titanium, particularly in samples processed via the BE route.

In this regard, laser surface modification proved to be highly effective in promoting phase homogenization within the modified layer.

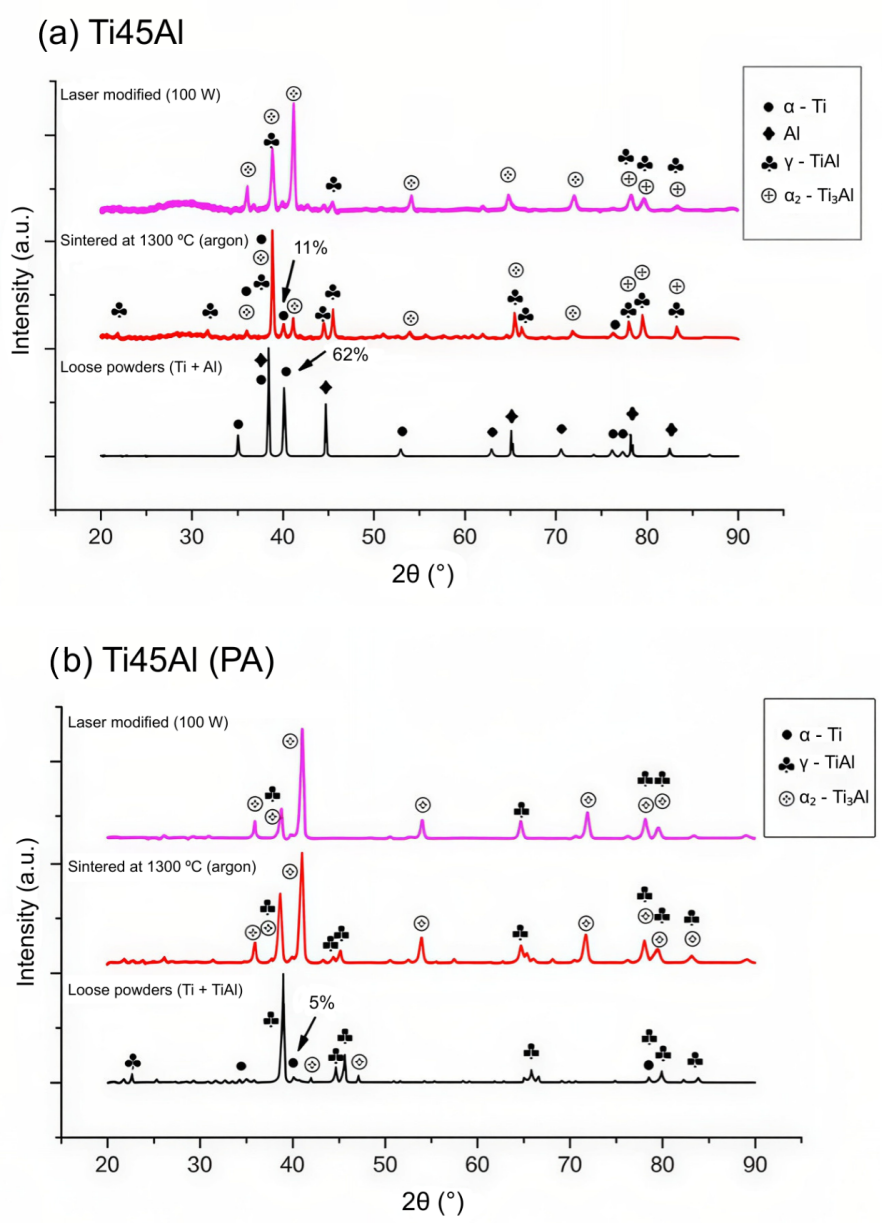

Figure 8. XRD patterns of Ti-45Al alloys produced by powder metallurgy using (**a**) BE and (**b**) PA powders, in the compacted, sintered, and laser-modified conditions.

Consistent with observations reported in previous studies [7,11], laser surface remelting was found to influence the kinetics of the eutectoid transformation ($\alpha \rightarrow \alpha_2 + \gamma$). The rapid thermal cycles associated with laser processing tend to suppress the formation of the γ phase, while promoting an increased fraction of the α_2 phase due to the enhanced $\alpha \rightarrow \alpha_2$ ordering transformation [42]. This behavior is associated with the high cooling rates and non-equilibrium conditions imposed during laser remelting.

Several studies have reported the presence of the β phase along grain boundaries in Ti-Al-based alloys, typically attributed to the addition of β-stabilizing elements such as Nb or Cr [7,23,40,42]. In the present study, since such alloying elements were not incorporated into the compositions, no evidence of β phase formation or other out-of-equilibrium phases was detected by XRD.

Figure 8 presents the XRD patterns obtained from the green compacts, sintered samples, and laser-modified layers of Ti-45Al alloys produced via the BE (Figure 8a) and PA (Figure 8b) routes. The diffraction results indicate that laser processing did not introduce additional phases beyond those expected from the Ti-Al equilibrium system under the investigated conditions.

A semi-quantitative analysis of the XRD peak intensities was performed to assess the phase evolution after laser processing further. In the BE-processed alloy (Figure 8a), reflections indexed to the α_2 phase show a noticeable increase in relative intensity, particularly the main peak near $2\theta \approx 41°$, accompanied by a decrease in the intensity of the main γ reflections. This trend suggests an increase in the relative fraction of the α_2 phase within the remelted layer. Based on the intensity of the peaks, the α_2 variation went from 15% (sintered) to 63% (laser-remelted) in the case of BE. In contrast, the PA-processed alloy (Figure 8b) exhibited a smaller yet noticeable variation in peak intensities, indicating a change of α_2 fractions from 62% (sintered) to 78% (laser-remelted). The relative changes in peak intensities suggest phase redistribution induced by the rapid thermal cycle associated with laser surface remelting.

In contrast to the present observations, Liu, Zhu, and Zhang [43] reported a reduction in the α_2 phase fraction in Ti-Al alloys subjected to high-temperature annealing followed by furnace cooling, highlighting the strong influence of thermal history on phase stability and transformation pathways.

3.4. Microindentation Results

Figure 9 shows representative loading–unloading curves obtained from microindentation tests performed on Ti-45Al samples in the conventionally sintered condition and after laser surface modification applied to previously sintered specimens. The laser-modified layers exhibit significantly lower penetration depths when compared to the sintered condition, indicating a clear enhancement in mechanical resistance. This behavior is primarily attributed to the increased local density, improved microstructural homogeneity, and pronounced microstructural refinement induced by the laser processing.

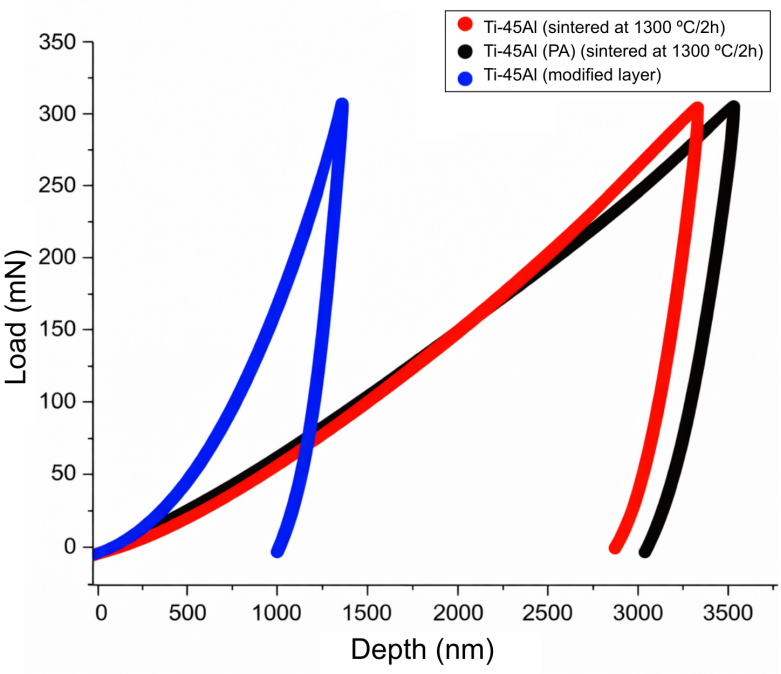

Figure 9. Representative loading–unloading curves obtained from microindentation tests performed on conventionally sintered samples and on the laser-modified layers of Ti-45Al-based alloys.

These improvements can be rationalized by classical strengthening mechanisms. The rapid solidification associated with laser surface remelting produces a refined microstructure, increasing grain-boundary density and restricting dislocation motion, consistent with the Hall–Petch effect [44]. In addition, the localized reduction in porosity increases the effective load-bearing area and reduces stress concentrations, resulting in higher elastic stiffness and resistance to plastic deformation.

In addition to densification effects, the increased fraction of the α_2 (Ti_3Al) phase identified in the laser-modified layers (Figure 8) is expected to contribute to the observed improvement in mechanical performance, since this phase is known to promote higher strength and hardness in Ti-Al-based alloys [7,8,42]. This strengthening effect arises because the α_2 (Ti_3Al) phase generally exhibits a more ordered and stiffer crystal structure compared to the γ-TiAl phase, which increases resistance to plastic deformation. The presence of a greater α_2 fraction can thus impede dislocation motion and intrinsically contribute to higher hardness and elastic modulus values in regions enriched in this phase, as observed in the laser-modified layers [45].

The elastic modulus and hardness values derived from the microindentation tests are summarized in Table 4, highlighting the influence of laser modification on the mechanical behavior of TiAl. Despite the limited number of indentations, the results showed consistent trends among the analyzed conditions.

Table 4. Elastic modulus and hardness values obtained from microindentation tests for conventionally sintered and laser-modified Ti-45Al-based alloys (mean ± standard deviation, n = 5).

Composition	Condition	Elastic Modulus (GPa)	Hardness (GPa)
Ti-45Al	Sintered	112 ± 9	4.0 ± 0.9
Ti-45Al	Laser-modified layer	188 ± 9	6.1 ± 0.2
Ti-45Al-2Co	Sintered	162 ± 8	5.8 ± 0.4
Ti-45Al-2Co	Laser-modified layer	182 ± 25	6.9 ± 0.2

For the Ti-45Al alloy, laser processing resulted in a substantial increase in elastic modulus and hardness, by approximately 69% and 50%, respectively, when compared to the conventionally sintered condition. Moreover, the Ti-45Al-2Co alloy exhibited an even more pronounced increase in hardness, suggesting that Co may act as an effective solid-solution strengthener in the laser-modified microstructure. The measured mechanical properties are consistent with values reported in the literature for laser-processed Ti-Al alloys [11].

It should be noted that the baseline mechanical properties discussed in this section correspond to conventionally sintered samples with relatively low densification, which is typical of pressure-less sintering without densification aids or post-sintering treatments. In contrast, relative densities in the range of 92–98% have been reported for γ-TiAl alloys processed under optimized sintering conditions (e.g., higher temperatures, extended dwell times, or hot isostatic pressing), generally resulting in significantly improved mechanical properties [46–48]. Therefore, the substantial improvements observed in the laser-modified layers primarily reflect localized densification and microstructural refinement relative to a porous substrate. Nevertheless, these findings demonstrate the effectiveness of laser surface remelting in enhancing the surface mechanical performance of powder-metallurgy TiAl alloys processed under representative conditions.

Complementary hardness measurements on individual microconstituents of the Ti-45Al-2Ni alloys sintered at 1300 °C indicate higher hardness values in Ni-rich regions when compared to the γ-TiAl and lamellar (Ti_3Al + TiAl) microstructures. Hardness values on the order of 7.2 GPa were measured in Ni-enriched areas, whereas the γ-TiAl phase

and lamellar regions exhibited values of approximately 2.9 GPa and 4.3 GPa, respectively. This trend is consistent with solid-solution strengthening effects associated with high local Ni concentrations and provides additional context for the hardness increase observed in laser-modified Ti-45Al-based alloys.

4. Conclusions

With the aim of enhancing densification, microstructural homogeneity, and refinement in TiAl, materials that pose significant challenges under conventional sintering routes, a laser surface modification was applied to both compacted and sintered alloys. The main conclusions can be summarized as follows:

- Laser surface modification effectively increased the local density of both green compacts and conventionally sintered samples of binary and ternary compositions, demonstrating its suitability as a post-processing route for TiAl;
- Laser processing promoted pronounced microstructural modifications, including an increased fraction of the α_2 (Ti_3Al) phase, a relative reduction in the γ (TiAl) phase, the formation of columnar grain structures, and the complete dissolution of residual elemental Ti;
- The green (compacted) condition played a key role in stress accommodation during laser processing, contributing to a reduced incidence of cracks and residual porosity in the modified layers;
- As a combined effect of increased densification and the higher α_2 phase fraction, the laser-modified layers exhibited a significant improvement in surface mechanical properties, particularly in terms of hardness. It should be noted that the baseline sintered samples in this study exhibited relatively high porosity compared to literature reports of optimized conventional sintering of TiAl alloys, where relative densities in the range of 95–97% are frequently achieved and are associated with correspondingly higher mechanical properties.

Author Contributions: W.M.: writing—original draft preparation, conceptualization, methodology, software, validation, formal analysis, investigation and data curation, J.V.V.: writing—review and editing, formal analysis; J.B.F.: writing—review and editing, investigation, and formal analysis. J.S.: writing—review and editing, resources, supervision, project administration, and funding acquisition. All authors have read and agreed to the published version of the manuscript.

Funding: This work was supported by the São Paulo Research Foundation (FAPESP) under Grant 2018/04564-0 and the Coordination for the Improvement of Higher Education Personnel (CAPES)—Finance Code 001.

Institutional Review Board Statement: Not applicable.

Informed Consent Statement: Not applicable.

Data Availability Statement: All data generated or analyzed in the present study are contained within the article.

Acknowledgments: The authors are grateful for the technical support provided by the staff of the Multi-User Materials Characterization Laboratory, University of Campinas, and the Research, Innovation and Development Center of Espírito Santo (CPID).

Conflicts of Interest: The authors declare no conflicts of interest.

References

1. McElroy, S.; Yang, D.; Reddy, R.G. Laser processing of titanium aluminides. *J. Mater. Eng. Perform.* **2000**, *9*, 506–515. [CrossRef]
2. Gibson, I.; Brent, S.; Rosen, D.W. *Additive Manufacturing Technologies*; Springer: New York, NY, USA, 2010.

3. Wu, Y.; Wang, H.; Ma, X.; Wang, J.; Cheng, F.; Han, J.; Cheng, X.; Li, A.; He, B. Fabrication of TiAl alloy with no multiple heat-affected bands using continuous direct energy deposition. *Mater. Lett.* **2020**, *281*, 128581. [CrossRef]
4. Gasper, A.N.D.; Catchpole-Smith, S.; Clare, A.T. In-situ synthesis of titanium aluminides by direct metal deposition. *J. Mater. Process. Technol.* **2017**, *239*, 230–239. [CrossRef]
5. Schimbäck, D.; Braun, J.; Leichtfried, G.; Clemens, H.; Mayer, S. Laser powder bed fusion of an engineering intermetallic TiAl alloy. *Mater. Des.* **2021**, *201*, 7–12. [CrossRef]
6. Zhang, X.; Mao, B.; Mushongera, L.; Kundin, J.; Liao, Y. Laser powder bed fusion of titanium aluminides: An investigation on site-specific microstructure evolution mechanism. *Mater. Des.* **2021**, *201*, 109501. [CrossRef]
7. Li, W.; Liu, J.; Wen, S.; Wei, Q.; Yan, C.; Shi, Y. Crystal orientation, crystallographic texture and phase evolution in the Ti-45Al-2Cr-5Nb alloy processed by selective laser melting. *Mater. Charact.* **2016**, *113*, 125–133. [CrossRef]
8. Gussone, J.; Garces, G.; Haubrich, J.; Stark, A.; Hagedorn, Y.-C.; Schell, N.; Requena, G. Microstructure stability of γ-TiAl produced by selective laser melting. *Scr. Mater.* **2017**, *130*, 110–113. [CrossRef]
9. Soliman, H.A.; Elbestawi, M. *Titanium Aluminides Processing by Additive Manufacturing—A Review*; Springer: Cham, Switzerland, 2022.
10. Tian, Y.S.; Chen, C.Z.; Li, S.T.; Huo, Q.H. Research progress on laser surface modification of titanium alloys. *Appl. Surf. Sci.* **2005**, *242*, 177–184. [CrossRef]
11. Xu, Z.; Ouyang, W.; Liu, Y.; Jiao, J.; Liu, Y.; Zhang, W. Effects of laser polishing on surface morphology and mechanical properties of additively manufactured TiAl components. *J. Manuf. Process.* **2021**, *65*, 51–59. [CrossRef]
12. Haponova, O.; Tarelnyk, V.; Tarelnyk, N.; Laponog, G. Investigation of Aluminum Electrospark Alloyed Coatings on Steels. *Metall. Mater. Trans. A* **2025**, *56*, 4204–4229. [CrossRef]
13. Deviatko, O.; Denisenko, M.; Kanivets, N.; Tuziuk, M. Electric Spark Alloying is an Effective Method of Surface Hardening of Metal Materials. In *Advanced Manufacturing Processes VII*; Lecture Notes in Mechanical Engineering; Springer: Cham, Switzerland, **2026**; pp. 414–426. [CrossRef]
14. Appel, J.F.; Paul, D.H.; Oehring, M. *Gamma Titanium Aluminide Alloys*; Wiley-VCH: Weinheim, Germany, 2011.
15. Clemens, H.; Heinrich, K. Processing and applications of intermetallic γ-TiAl-based alloys. *Adv. Eng. Mater.* **2000**, *2*, 551–570. [CrossRef]
16. Kothari, K.; Radhakrishnan, R.; Wereley, N.M. Advances in gamma titanium aluminides and their manufacturing techniques. *Prog. Aerosp. Sci.* **2012**, *55*, 1–16. [CrossRef]
17. Genc, O.; Unal, R. Development of gamma titanium aluminide (γ-TiAl) alloys: A review. *J. Alloys Compd.* **2022**, *929*, 167262. [CrossRef]
18. Alves, J.; Quaglio, L.; Monfardini, W.A.; Soyama, J. Sinterability and microstructure evolution of powder metallurgy processed titanium aluminides. *Mater. Sci. Technol.* **2022**, *39*, 42–49. [CrossRef]
19. Sina, H.; Iyengar, S. Reactive synthesis and characterization of titanium aluminides produced from elemental powder mixtures. *J. Therm. Anal. Calorim.* **2015**, *122*, 689–698. [CrossRef]
20. Ye, S.; Hao, H.; Mo, W.; Yu, K.; Liu, L.; Deng, C.; Yu, P. Effects of cold compacting pressure on the expansion behavior of Ti-48Al during sintering. *J. Alloys Compd.* **2016**, *673*, 399–404. [CrossRef]
21. Jiang, Y.; He, Y.H.; Xu, N.P.; Zou, J.; Huang, B.Y.; Liu, C.T. Effects of the Al content on pore structures of porous Ti-Al alloys. *Intermetallics* **2008**, *16*, 327–332. [CrossRef]
22. Yang, J.B.; Hwang, W.S. The preparation of TiAl-based intermetallics from elemental powders through a two-step pressureless sintering process. *J. Mater. Eng. Perform.* **1998**, *7*, 385–392. [CrossRef]
23. Gussone, J.; Hagedorn, Y.-C.; Gherekhloo, H.; Kasperovich, G.; Merzouk, T.; Hausmann, J. Microstructure of γ-titanium aluminide processed by selective laser melting at elevated temperatures. *Intermetallics* **2015**, *66*, 133–140. [CrossRef]
24. Harada, Y.; Ishida, Y.; Miura, D.; Watanabe, S.; Aoki, H.; Miyasaka, T.; Shinya, A. Mechanical properties of selective laser sintering pure titanium and Ti-6Al-4V, and its anisotropy. *Materials* **2020**, *13*, 5081. [CrossRef]
25. Yan, Q.; Chen, B.; Kang, N.; Lin, X.; Lv, S.; Kondoh, K.; Li, S.; Li, J.S. Comparison study on microstructure and mechanical properties of Ti-6Al-4V alloys fabricated by powder-based selective laser melting and sintering methods. *Mater. Charact.* **2020**, *164*, 110358. [CrossRef]
26. Fogagnolo, J.B.; Rodrigues, A.V.; Lima, M.S.F.; Amigó, V.; Caram, R. A novel proposal to manipulate the properties of titanium parts by laser surface alloying. *Scr. Mater.* **2013**, *68*, 471–474. [CrossRef]
27. Anjos, S.d.; da Costa, F.H.; Sallica-Leva, E.; Caram, R.; Amigó, V.; Fogagnolo, J.B. Laser surface alloying applied on Ti-3Mo and Ti-10Nb sintered parts. *Surf. Coatings Technol.* **2021**, *407*, 126773. [CrossRef]
28. de Carvalho, L.R.A.; Sallica-Leva, E.; Encinas, E.R.; Fogagnolo, J.B. Less-rigid coating in Ti obtained by laser surface alloying with Nb. *Surf. Coatings Technol.* **2018**, *346*, 19–28. [CrossRef]
29. Zhu, L.; Xue, P.; Lan, Q.; Meng, G.; Ren, Y.; Yang, Z.; Xu, P.; Liu, Z. Recent research and development status of laser cladding: A review. *Opt. Laser Technol.* **2021**, *138*, 106915. [CrossRef]

30. da Costa, F.H.; Sallica-Leva, E.; Mello, M.G.; Amigó, V.; Caram, R.; Fogagnolo, J.B. Stiffness and hardness gradients obtained by laser surface treatment of aged β-Ti alloys: The role of ω phase. *Surf. Coatings Technol.* **2023**, *467*, 129697. [CrossRef]
31. Thijs, L.; Verhaeghe, F.; Craeghs, T.; Humbeeck, J.V.; Kruth, J.-P. A study of the microstructural evolution during selective laser melting of Ti-6Al-4V. *Acta Mater.* **2010**, *58*, 3303–3312. [CrossRef]
32. Xu, W.; Brandt, M.; Sun, S.; Elambasseril, J.; Liu, Q.; Latham, K.; Xia, K.; Qian, M. Additive manufacturing of strong and ductile Ti-6Al-4V by selective laser melting via in situ martensite decomposition. *Acta Mater.* **2015**, *85*, 74–84. [CrossRef]
33. Oliver, W.; Pharr, G. An improved technique for determining hardness and elastic modulus using load and displacement sensing indentation experiments. *J. Mater. Res.* **1992**, *7*, 1564–1583. [CrossRef]
34. *ASTM E2546-15*; Standard Practice for Instrumented Indentation Testing. ASTM International: West Conshohocken, PA, USA, 2015. [CrossRef]
35. *ASTM B933-14*; Standard Test Method for Microindentation Hardness of Powder Metallurgy (PM) Materials. ASTM International: West Conshohocken, PA, USA, 2014. [CrossRef]
36. Liu, H.W.; Plucknett, K.P. Titanium aluminide (Ti-48Al) powder synthesis, size refinement and sintering. *Adv. Powder Technol.* **2017**, *28*, 314–323. [CrossRef]
37. Xia, Y.; Schaffer, G.B.; Qian, M. The effect of a small addition of nickel on the sintering, sintered microstructure, and mechanical properties of Ti-45Al-5Nb-0.2C-0.2B alloy. *J. Alloys Compd.* **2013**, *578*, 195–201. [CrossRef]
38. Xia, Y.; Yu, P.; Schaffer, G.B.; Qian, M. Cobalt-doped Ti-48Al-2Cr-2Nb alloy fabricated by cold compaction and pressureless sintering. *Mater. Sci. Eng. A* **2013**, *574*, 176–185. [CrossRef]
39. *ASTM B962-13*; Standard Test Methods for Density of Compacted or Sintered Powder Metallurgy (PM) Products Using Archimedes' Principle. ASTM International: West Conshohocken, PA, USA, 2013. [CrossRef]
40. Li, W.; Liu, J.; Zhou, Y.; Wen, S.; Wei, Q.; Yan, C.; Shi, Y. Effect of substrate preheating on the texture, phase and nanohardness of a Ti-45Al-2Cr-5Nb alloy processed by selective laser melting. *Scr. Mater.* **2016**, *118*, 13–18. [CrossRef]
41. McCullough, C.; Valencia, J.J.; Levi, C.G.; Mehrabian, R. Phase equilibria and solidification in Ti-Al alloys. *Acta Metall.* **1989**, *37*, 1321–1336. [CrossRef]
42. Clemens, H.; Chladil, H.F.; Wallgram, W.; Zickler, G.A.; Gerling, R.; Liss, K.-D.; Kremmer, S.; Güther, V.; Smarsly, W. In and ex situ investigations of the β-phase in a Nb- and Mo-containing γ-TiAl-based alloy. *Intermetallics* **2008**, *16*, 827–833. [CrossRef]
43. Liu, Z.; Zhu, X.; Zhang, Y. Effect of annealing treatment on microstructure and tensile properties of Ti-48Al-2Cr-5Nb alloy fabricated by laser additive manufacturing. *Opt. Laser Technol.* **2022**, *155*, 108412. [CrossRef]
44. Huang, Y.-C.; Su, C.-H.; Wu, S.-K.; Lin, C. A Study on the Hall-Petch Relationship and Grain Growth Kinetics in FCC-Structured High/Medium Entropy Alloys. *Entropy* **2019**, *21*, 297. [CrossRef]
45. Avdeeva, V.; Bazhina, A.; Antipov, M.; Stolin, A.; Bazhin, P. Relationship between Structure and Properties of Intermetallic Materials Based on γ-TiAl Hardened In Situ with Ti_3Al. *Metals* **2023**, *13*, 1002. [CrossRef]
46. Yan, M.; Yang, F.; Lu, B.; Chen, C.; Sui, Y.; Guo, Z. Microstructure and Mechanical Properties of High Relative Density γ-TiAl Alloy Using Irregular Pre-Alloyed Powder. *Metals* **2021**, *11*, 635. [CrossRef]
47. Monfardini, W.A.; Soyama, J. Microstructural Formation and Creep Resistance of Sintered Titanium Aluminides with Co and Ni Addition. *Mater. Res.* **2025**, *28*, e20250093. [CrossRef]
48. Quaglio, L.; Monfardini, W.A.; Soyama, J. Sintering titanium aluminides with Co addition. *Mater. Sci. Forum* **2025**, *1146*, 13. [CrossRef]